Microembossing of ultrafine grained Al: microstructural analysis and finite element modelling

2010 J. Micromech. Microeng. 20 105002

(http://iopscience.iop.org/0960-1317/20/10/105002)

J. Micromech. Microeng. **20** (2010) 105002 (14pp) doi:10.1088/0960-1317/20/10/105002

Microembossing of ultrafine grained Al: microstructural analysis and finite element modelling

Xiao Guang Qiao[1], Mamadou T Bah[2], Jiuwen Zhang[1,3], Nong Gao[1], Zakaria Moktadir[4], Michael Kraft[4] and Marco J Starink[1]

[1] Materials Research Group, School of Engineering Sciences, University of Southampton, Southampton SO17 1BJ, UK
[2] Bioengineering Science Research Group, School of Engineering Sciences, University of Southampton, Southampton SO17 1BJ, UK
[3] School of Materials Science and Engineering, Dalian University of Technology, 110685, Liaoning, People's Republic of China
[4] School of Electronics and Computer Science, University of Southampton, Southampton SO17 1BJ, UK

E-mail: xgqiao@126.com, M.J.Starink@soton.ac.uk, N.Gao@soton.ac.uk, mtb@soton.ac.uk, jiuwenzh@yahoo.com.cn, zm@ecs.soton.ac.uk and mk1@ecs.soton.ac.uk

Received 5 May 2010, in final form 19 July 2010
Published 1 September 2010
Online at stacks.iop.org/JMM/20/105002

Abstract
Ultra-fine-grained (UFG) Al-1050 processed by equal channel angular pressing and UFG Al–Mg–Cu–Mn processed by high-pressure torsion (HPT) were embossed at both room temperature and 300 °C, with the aim of producing micro-channels. The behaviour of Al alloys during the embossing process was analysed using finite element modelling. The cold embossing of both Al alloys is characterized by a partial pattern transfer, a large embossing force, channels with oblique sidewalls and a large failure rate of the mould. The hot embossing is characterized by straight channel sidewalls, fully transferred patterns and reduced loads which decrease the failure rate of the mould. Hot embossing of UFG Al–Mg–Cu–Mn produced by HPT shows a potential of fabrication of microelectromechanical system components with micro channels.

(Some figures in this article are in colour only in the electronic version)

1. Introduction

Microchannel-patterned devices are extensively applied in microelectromechanical systems (MEMS) such as optical switches, microreactors and micro heat exchangers. One way to fabricate such devices is to perform deep reactive ion etching (DRIE) on silicon wafers to get the components with micro scaled patterns [1]. The patterned silicon chips can be used as individual microparts or micro moulds allowing a polymer to be embossed [2]. However, silicon and polymers cannot meet the requirements of some applications. For instance, the materials inside micro heat exchangers are required to have a high thermal conductivity. The potential materials to replace silicon and polymers are metals, which generally have low thermal resistance and preferentially low cost metals and alloys such as Cu and Al. These metals have been used extensively to fabricate traditional heat exchangers. Additionally, steel and titanium have been used [3–6] to fabricate micro heat exchangers with channel size in a scale of hundreds of micrometres by diamond machining. As we discussed before [7] a range of processes may be considered for producing microchannel-patterned devices (LIGA, diamond cutting, microextrusion, RIE, DRIE). We will here focus on micro-embossing.

Embossing of polymers occurs at a temperature between the glass transition temperature and the melting temperature. The dominant mechanism of deformation is visco-elastic flow. The processing of metallic alloys is different and parameters cannot be simply adopted from polymer embossing. Otto *et al* [8] attempted to fabricate optical components with

micro channels of a few micrometres size by cold embossing using conventional coarse-grained aluminium. The embossed surface showed uneven and rounded planks with ridges. Jiang *et al* [9] used a silicon mould with parallel channels of 11.7 μm width to emboss a coarse-grained pure aluminium of 2 mm $\times$ 2 mm area at ambient temperature. A very high mould failure rate was observed, which was ascribed to misalignment of embossing [9]. Böhm *et al* [10] studied straight channels and complex structures fabricated by cold embossing and embossing at elevated temperatures. A silicon die in various relatively fine grained materials (grain size >3 μm) was used, including pure aluminium, stainless steel, pure copper and brass CuZn37. The minimum structure width was 10 μm. The cold embossed surface showed a better quality than that in their previous attempts [8] due to the finer grains, although the channel edges were still rounded [10]. In order to achieve complete moulding of the structure, a compressive stress much higher than the yield stress proved necessary. A significant lower loading force was observed during complex structure embossing of the Zn78Al22 alloys at elevated temperature. However, the channel edges were still rounded due to superplastic deformation by grain boundary sliding and grain rotation [10]. The problems reported in the literature are thought to be related, amongst others, to the difficulty in reliably embossing metals with conventional microstructures. Our recent study [7] indicated that refining the grain size prior to embossing improves the process and quality of the embossed surface. It was particularly shown that hot embossing of a fine grained Al-1050 alloy provided a smooth embossed surface with fully transferred pattern and a low failure rate of the mould, while hot embossing on a coarse-grained Al-1050 resulted in a rougher surface with shear bands [7].

In severe plastic deformation (SPD), conventional microstructures materials are changed to submicron or nano-scaled ones [11–13]. Equal channel angular pressing (ECAP) is one of the most effective processing methods among the group of SPD methods [14, 15]. It can be repeatedly performed on a single specimen because the specimen's cross-sectional shape does not change during ECAP processing. The produced materials with submicron or nano-scaled grains are of low cost, low porosity, low oxide content and are safe compared to their counterparts obtained using gas condensation and mechanical alloying [11, 15]. Although extensive research has been carried out on the microstructure and properties of ECAP processed alloys during the last decade [15–17], the application of ECAP processed materials and the exploitation of the ultra-fine grain structure are still of great interest to the research community. High pressure torsion (HPT) is another SPD method, which differs from conventional torsion by imposing a large hydrostatic pressure of up to several GPa during processing [18]. The HPT sample has a disc shape, typically of 10–20 mm diameter and 0.2–0.9 mm thickness [19, 20]. During HPT, the sample is put into an almost closed die and a compressing force is imposed on the sample. Then, one or both contact platens impose a shear strain in the sample by rotating one of the platens (or both in opposite directions). A large accumulated strain and grain refinement can be achieved during several turns of rotations. This process can substantially refine the grain size, for instance, the grain size of an Al–3%Mg–0.2%Sc can be refined to 0.15 μm after six turns of rotation at room temperature using a 6 GPa pressure [21]. HPT is more powerful in grain refinement than ECAP because a more severe strain can be created in a shorter processing time and strain can be generated without interruption. However, the size of HPT samples, although large enough for most MEMS applications, is generally much smaller than ECAP samples.

A number of studies reported the moulding response of the Al material using both experimental and numerical techniques [9, 22–25]. In the elastic regime, the stress distribution can be exactly derived for both single and periodic punch cases [25, 26]. In the plastic regime, a main challenge is the validation of moulding models based on contact mechanics and moulding experiments. For a perfectly plastic substrate occupying a unit of the periodic array of strip punches, the frictionless moulding response can be analytically derived [26]. Furthermore, for the simulation of both elasto-plastic and perfectly plastic indentation, the finite element (FE) method can be used to compute the strain distribution throughout the area of the yield region. Jiang [26], for example, used a calibrated FE mesh in the elastic contact regime against the known analytic solution for the Al material indented by a periodic array of frictionless flat punches. This calibrated mesh was then used to track the indentation process in the elasto-plastic regime.

In the present study, the embossing process is evaluated using both experimental measurements and FE modelling. Following on from our initial work on the processing of metallic foils with features at the scale of 5–50 μm [7] using ultra-fine-grained (UFG) Al processed by ECAP, this study focuses on the plastic flow of the UFG Al during the embossing process. The topography and the cross-section of embossed channels are characterized by scanning electron microscopy (SEM) and focused ion beam (FIB). In addition, an FE model of an elasto-plastic Al substrate indented by a single punch with two small rounded corners is developed to simulate the embossing process.

2. Materials and methods

2.1. Materials and processing

The present study was carried out on an Al-1050 and an Al–Mg–Cu–Mn alloy. Al-1050 is commercial purity aluminium with composition Al–0.18Fe–0.12Si (in wt%) with further minor impurities. (Note that Fe and Si are the two most abundant impurities in aluminium, the price of Al increase strongly with increasing purity.) The supplied Al-1050 rod is an extrusion of diameter 9.53 mm, which was cut to ECAP billets of length 65 mm. ECAP was performed at room temperature. For ECAP processing, the lubricated billet was pressed through a die containing two channels, equal in cross-section (9.7 mm diameter), intersecting at an angle $\Phi = 90^\circ$ (figure 1(*a*)). The equivalent strain after one pass of ECAP is about 1 [27]. The ECAP process was conducted up to 12

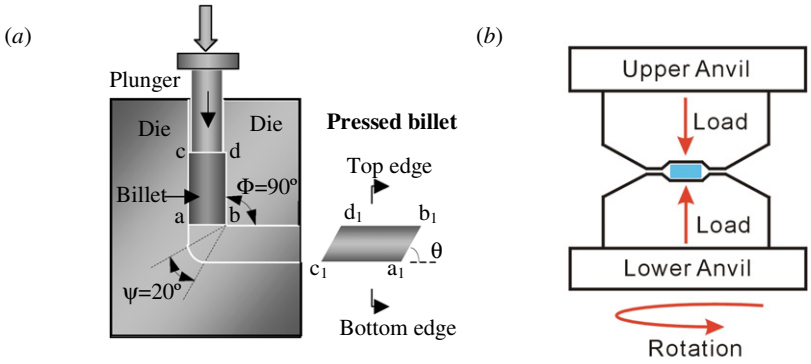

Figure 1. Principle of SPD: (*a*) ECAP, (*b*) HPT.

passes; further details on ECAP processing are provided in [28].

The Al–Mg–Cu–Mn alloy with composition Al–2.90Mg–0.40Cu–0.25Mn–0.19Fe-0.15Si (in wt%) was produced by direct chill casting, then preheated and homogenized at 540 °C, hot rolled down into 5 mm thickness, solution treated at 500 °C for 20 min, and cold rolled to 10% reduction (details are provided in [29]). The rolled plate was cut to HPT disc-shaped samples of 10 mm diameter and 0.8 mm thickness. The disc was HPT processed for five turns at room temperature under a pressure of 3 GPa (see [30] for further details on HPT processing).

The ECAP processed billet was machined along the longitudinal direction to 1 mm thick disc-shaped samples for embossing. The circular surface of discs, including Al-1050 cut from the ECAP processed billet and Al–Mg–Cu–Mn processed by HPT, was ground by abrasive papers up to 1200 grits and then polished to the mirror-like surface. The embossing process was carried out on the circular surface by the micro silicon die, i.e. a square plate of 14 mm side length and 0.5 mm thickness. The pattern on the centre of the micro silicon die is 10 mm long and 10 mm wide consisting of a series of parallel straight channels of 10 μm depth and 3–50 μm width with the same size grating. The micro silicon die was fabricated by DRIE (see [7] for more details). The SEM image of the micro silicon die (figure 2) shows that the channel bottom is smooth. The measured depth of the channel is on average 10.03 μm.

The embossing process was carried out at ambient temperature and 300 °C on a 9510 Instron testing machine with maximum capacity of 10 kN (see figure 3). Platens and fixture were specially designed to fit the machine. A heating system and a cooling unit were specially designed to fit the machine. Embossing forces of 5 kN, 7 kN and 9 kN were used for cold embossing and a force of 3 kN was applied during embossing at 300 °C with a loading rate of 50 N s^{-1}, then held for 300 s. For hot embossing, the demoulding was performed at room temperature.

2.2. *Characterization methods*

Electron backscattered diffraction (EBSD) was used to characterize the microstructure as well as grain and subgrain boundary misorientation distribution in UFG Al-1050. For sample preparation, the surface of cross-section was first mechanically ground up to 4000 grit SiC paper, then electropolished employing an electrolyte composed of 33 vol% nitric acid and 67 vol% methanol. The electropolishing was carried out with a dc voltage of 20–30 V for 30 s at −30 °C. The equipment used was a JEOL JSM6500F thermal field emission gun scanning electron microscope (FEG–SEM) equipped with an HKL EBSD detector and the HKL Channel 5 software. The SEM accelerating voltage was set to 15 kV. The step size was 0.1 μm.

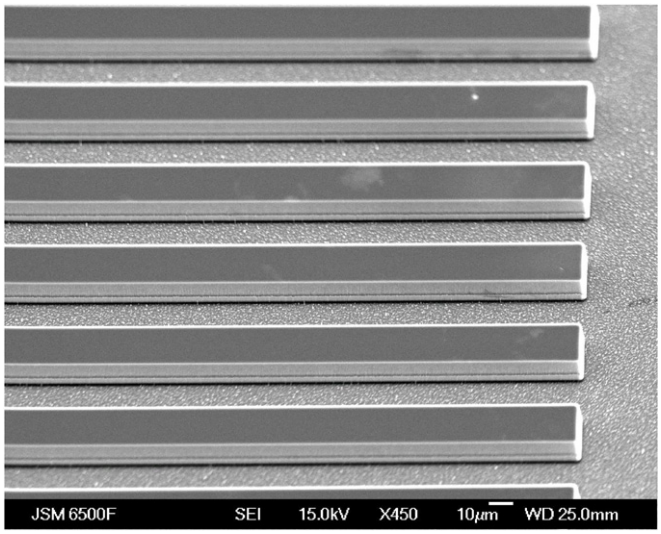

Figure 2. SEM image of a micro silicon die with the channel depth of 10 μm and width of 25 μm.

The FEG–SEM and an Olympus BH-2 optical microscope (OM) equipped with a Prosilica digital CCD camera were used to observe the cross-section and embossed surface of the UFG aluminium foils. A Carl Zeiss XB1540 focussed ion beam (FIB) was used to characterize the microstructure on the cross-section of the embossed foil. The FIB was operated at 30 kV with an ion beam current of 200 pA. For sample preparation, the embossed Al foils were mounted in transparent resin, where the longitudinal direction of channels on the circular surface of the embossed foils was perpendicular to the bottom flat surface of the mounted sample. The mounted sample was

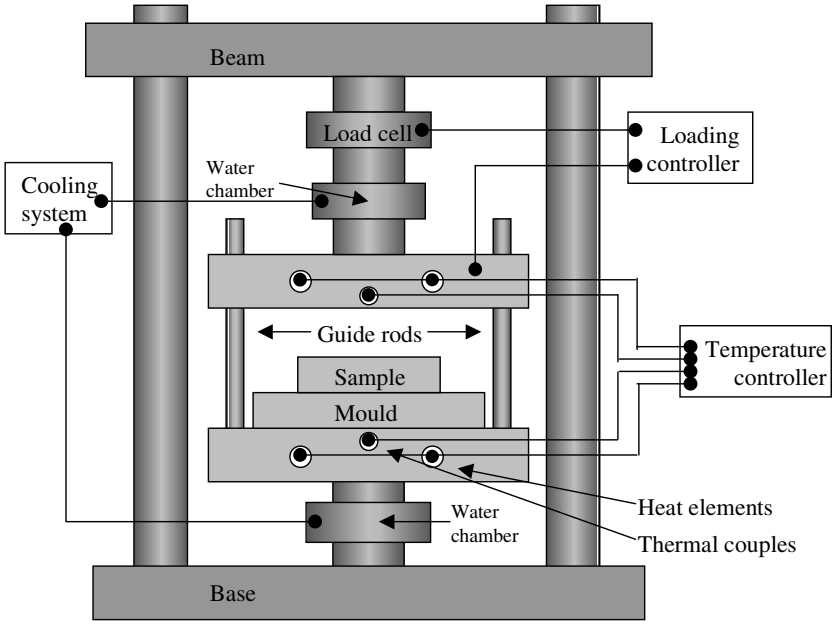

Figure 3. Sketch of the embossing setup showing the main components.

then ground by SiC paper up to 4000 grit followed by polishing using 1 μm diamond paste and fine polishing using Struers OP-S suspension until a clear profile of microchannels was observed under an optical microscope. Finally, the embossed foils were gently taken out from the resin and FIB milling was performed on the polished cross-section.

Microhardness was tested on an MHT-1 model micro Vickers hardness tester. For ECAP processed samples, five hardness values were measured on the cross-section at the centre area. For HPT processed samples, five hardness values were measured on the circular surface of the disc of 3 mm away from the centre. A force of 300 g was applied and held for 15 s.

2.3. FE modelling

The FE method was used to study the behaviour of an elasto-plastic Al substrate in a state of plane strain, indented by a single punch. Figure 4 shows the cross-section of the considered indentation geometry. The punch has a flat section of length $l = 12$ μm and width $w = 10$ μm. The bottom right edge of the punch has a round corner of radius $r = 0.5$ μm. The Al substrate has a rectangular cross-section of length $L = 20$ μm and width $W = 10$ μm. We first checked whether there was much difference in describing the punch as a rigid body or a linear elastic body. Differences were very small, and hence we decided to use the more computationally efficient rigid body description. ANSYS12 [31] was used to non-uniformly discretize the Al substrate with eight-node quadrilateral elements (PLANE183). These elements have two degrees-of-freedom at each node, i.e. translations in the x- and y-directions and have both plasticity and large strain capabilities. Mesh element distortion can prohibit an accurate prediction of large deformations and convergence of FE contact solution. Therefore, the mesh was deliberately made fine enough near the edge of contact (see figure 4). This guaranteed that the FE simulations did not terminate because of a mesh distortion. 2D three-node surface-to-surface elements (CONTA172) were used to model frictional contact between the rigid target surface (TARGE169) overlaid on the punch and the deformable Al substrate.

The boundary conditions for the Al substrate were as follows: no displacement in x-direction for nodes on the left and right edges (a) and fixed bottom end (b) (see figure 4). The entire rigid body punch was pressed into the elasto-plastic slab by applying a displacement of 5 μm and contacting the indented Al material over a width of 10 μm. Three true stress–strain curves, representing three microstructure/processing conditions, were considered for analysis. Condition 1 corresponds to conventional Al-1050 deforming at $T = 20$ °C under compressive loading, data are obtained from [32]. Condition 2 corresponds to UFG Al-1050 deforming at $T = 20$ °C, tensile data are taken from [33] for UFG Al–1 wt% Mg. Condition 3 corresponds to UFG Al-1050 deforming at $T = 300$ °C, stress–strain response is estimated using tensile test data of Al–1 wt% Mg by assuming that the small difference in composition (99.5 versus 99.0 wt% Al) and grain size do not significantly influence the deformation behaviour at 300 °C. Figure 5 displays these stress–strain curves. For each of these three stress–strain curves, ANSYS12 [31] was used to read a data table and assign the material properties to the indented Al material.

Young's modulus is $E = 69$ GPa and Poisson's ratio is $\nu = 0.33$. The entire FE model consists of 14 632 nodes and 4950 elements at $T = 20$ °C before ECAP, 13 047 nodes and 4415 elements at $T = 20$ °C after ECAP and 13 037 nodes and 4276 elements at $T = 300$ °C after ECAP. Mesh convergence studies were conducted to select the appropriate mesh size for each condition. A contact stiffness factor and a penetration tolerance of 1 and 0.1, respectively, were used for all analyses. Convergence was achieved using a coefficient

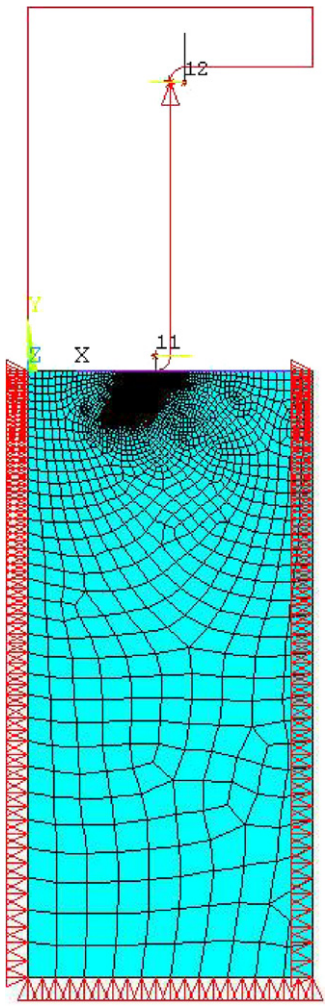

Figure 4. Finite element mesh of indentation assembly and boundary conditions.

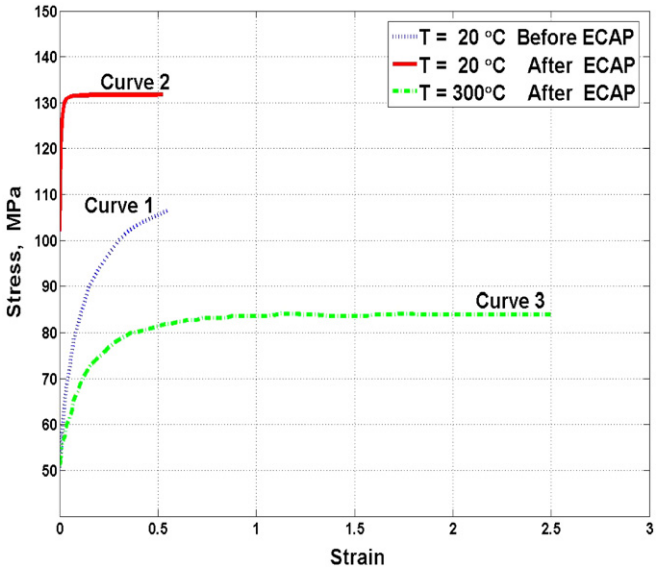

Figure 5. Stress–strain curves for indented Al-1050 at 20 °C before ECAP, 20 °C after ECAP and 300 °C after ECAP.

of friction of 0.05, which was subsequently adopted for all simulations. The coefficient of friction can only be an estimate. Jiang [26] assumed frictionless contact although a higher coefficient of friction of 0.7 was estimated. However, as stated by Jiang [26], 'because this is an estimate, a zero coefficient of friction was also taken to gauge the effects of friction and to access how critical is the accuracy of this estimate'. In the present study, a value of 0.05 was considered acceptable to achieve convergence and simulate the contact mechanics between the rigid punch and the indented material. Also, the difference in results obtained using coefficients of friction of 0 and 0.05 was found negligible.

The nonlinear problem was solved iteratively; the actual total number of substeps (subloads) required for convergence was 2081, 4540 and 5844 for the conditions 1, 2 and 3, respectively. The maximum number of equilibrium iterations for each substep was set to 100. The FE models were run on a dual processor XP workstation. The run times were 4.2, 13.5 and 8.71 CPU hours for conditions 1, 2 and 3, respectively. Once the convergence was achieved, contact results were post processed and the distribution of equivalent plastic strains (a measure of the intensity of plastic strain), Von Mises stresses and displacements in the Al substrate were analysed.

3. Results

3.1. Microstructure and hardness of the UFG Al-1050 and Al–Mg–Cu–Mn

Figure 6(*a*) shows the microstructure of the Al-1050 alloy after 12 passes of ECAP as determined by EBSD. The grey fine (dark thick) lines represent low angle grain boundaries of which the misorientation angle is between 2° and 15° (greater than 15°). Misorientations angles less than 2° were ignored. The average grain size defined by the mean linear intercept length was 0.88 μm after 12 passes of ECAP. The average Vickers hardnesses of Al-1050 are 43 Hv, 44 Hv, 48 Hv, 51 Hv and 51 Hv after 1, 2, 4, 8 and 12 passes of ECAP, respectively.

Figure 6(*b*) shows the microstructure of the Al–Mg–Cu–Mn alloy determined by FIB. It was processed by five turns of HPT following by annealing at 300 °C for 15 min. The FIB image was taken at the area close to the sample edge, in which grains were shown due to an orientation contrast. The average grain size measured in figure 6(*b*) is around 0.8 μm, which does not show a significant increase during anealling. Typically, the grain size of the Al–3wt%Mg–0.2wt%Sc alloy after the HPT process measued by TEM is around 0.2 μm [34]. The average Vickers hardness was measured to be 220 Hv in the periphery of the HPT processed disc.

3.2. Microstructure of the cross-section of cold embossed foils

The pattern of the micro silicon die failed to be transferred to the Al–Mg–Cu–Mn alloy by cold embossing because the hardness of the Al–Mg–Cu–Mn alloy after HPT processing was too large. For Al-1050 processed ECAP, the micro channels of the micro silicon die were partly transferred. For instance, one third of the foil surface was embossed when the embossing force was set at 5 kN. Figure 7 shows the optical

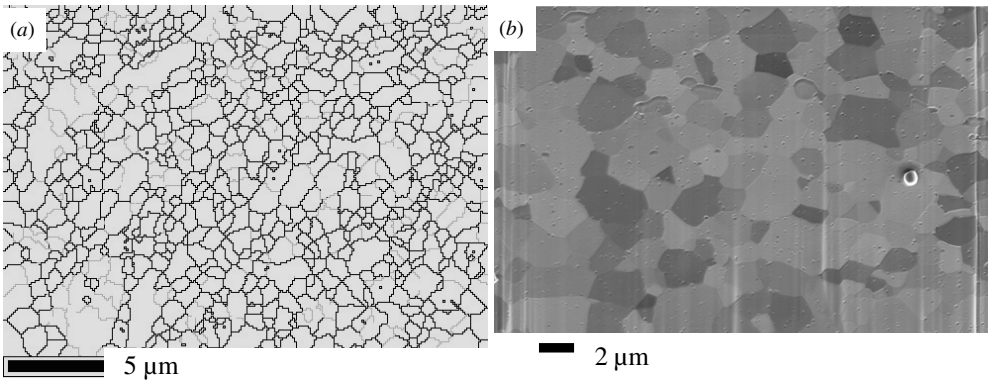

Figure 6. Microstructure of Al alloys before embossing (*a*) EBSD analysis of Al-1050 processed by 12 passes of ECAP; (*b*) FIB image of Al–Mg–Cu–Mn processed by five turns of HPT followed by annealing at 300 °C for 15 min.

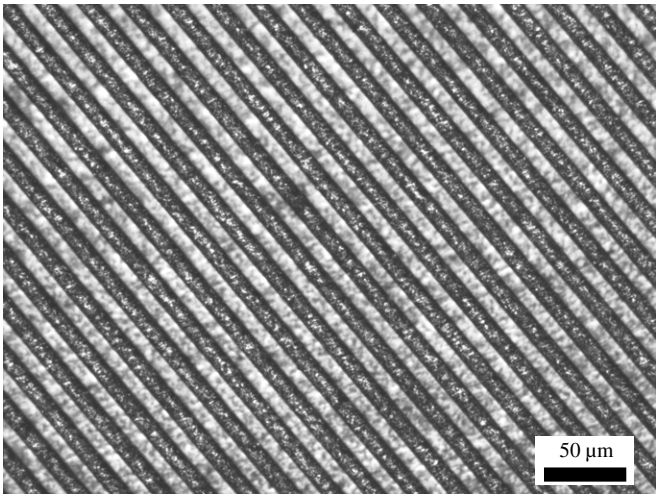

Figure 7. Optical micrograph of the embossed topography of the UFG Al-1050 foil after two passes of ECAP. The embossing force was 5 kN.

microscopy (OM) image of the embossed area of the foil. The channels on the micro silicon die were fully transferred to the foil surface.

The profile of microchannels of the eight passes of ECAP-processed Al-1050 (figure 8(*b*)) is sharper than that of the two passes of ECAP-processed Al-1050 (figure 8(*a*)). This is because the grain size of Al-1050 after eight passes of ECAP is smaller and grains are equiaxed [7]. However, the sidewalls of the microchannel in both embossed Al-1050 foils show an inclined angle to the channel bottoms, which causes demoulding to be difficult. Note that the bright contaminator at the bottom left of the sidewall in figure 8(*a*) is irremovable resin. This phenomenon is also predicted by FE modelling (see section 3.5).

Figures 8(*a*) and (*b*) show the cross-section of cold embossed Al-1050 foils processed by two and eight passes of ECAP, respectively. In figure 8(*a*), the microstructure at the centre of the cross-section retains the typical microstructure of Al-1050 after two passes of ECAP, i.e. many shear bands are inclined at an angle of around 45° to the ECAP pressing direction; but near the top surface (where strain is most intense, see section 3.5), the shear bands are rotated and refined to equiaxed grains. In figure 8(*b*), the microstructure does not show any difference between the centre and the edges. They are all equiaxed grains, which are a typical microstructure of Al-1050 after a large number of passes of ECAP.

3.3. Microstructure of hot embossed foils

Embossing at 300 °C led to the whole surface of both Al-1050 and Al–Mg–Cu–Mn imprinted. Figure 9(*a*) shows a typical SEM image of the surface of the UFG Al-1050 alloy foil embossed at 300 °C. The flake-like contaminants are MoS_2 used as solid lubricants. Figure 9(*b*) is a SEM image of the UFG Al–Mg–Cu–Mn foil embossed at 300 °C. The scratched channel tops are observed and the scratched marks remain on the same side of the channel tops. This phenomenon is observed on the channel top with other channel sizes. Figure 9(*c*) shows the topography of the hot embossed Al–Mg–Cu–Mn foil with channels of 25 μm width and 10 μm depth. The scratched channel top is clearly observed. The scratches occur in the same direction, indicating that they were not caused by vibration during demoulding. Figure 9(*d*) is an enlarged image of figure 9(*c*).

Cross-sections of Al-1050 and Al–Mg–Cu–Mn, embossed at 300 °C, are shown in figure 10. Channels sidewalls of both alloys are straight, which is beneficial to demoulding. However, the channel edges of both alloys are not perfectly sharp. The grain size (about 1 μm) in figure 10(*b*) is significantly smaller than the channel size (25 μm wide and 10 μm deep), but the channel edges are still rounded with an arc radius of about 10 μm. A similar large arc radius of rounded channel edges is observed in figure 10(*c*), where the channels are 50 μm wide and 10 μm deep. The above problems indicate that in hot embossing, parameters such as temperature, load, loading rate and holding time need further optimizing for each alloy.

3.4. FE modelling

The contour plot of nodal displacement in the *x*- and *y*-directions for the three specified conditions (figure 11) reveals that there is little difference between the three cases. The highest *x*-displacements were found near the bottom round

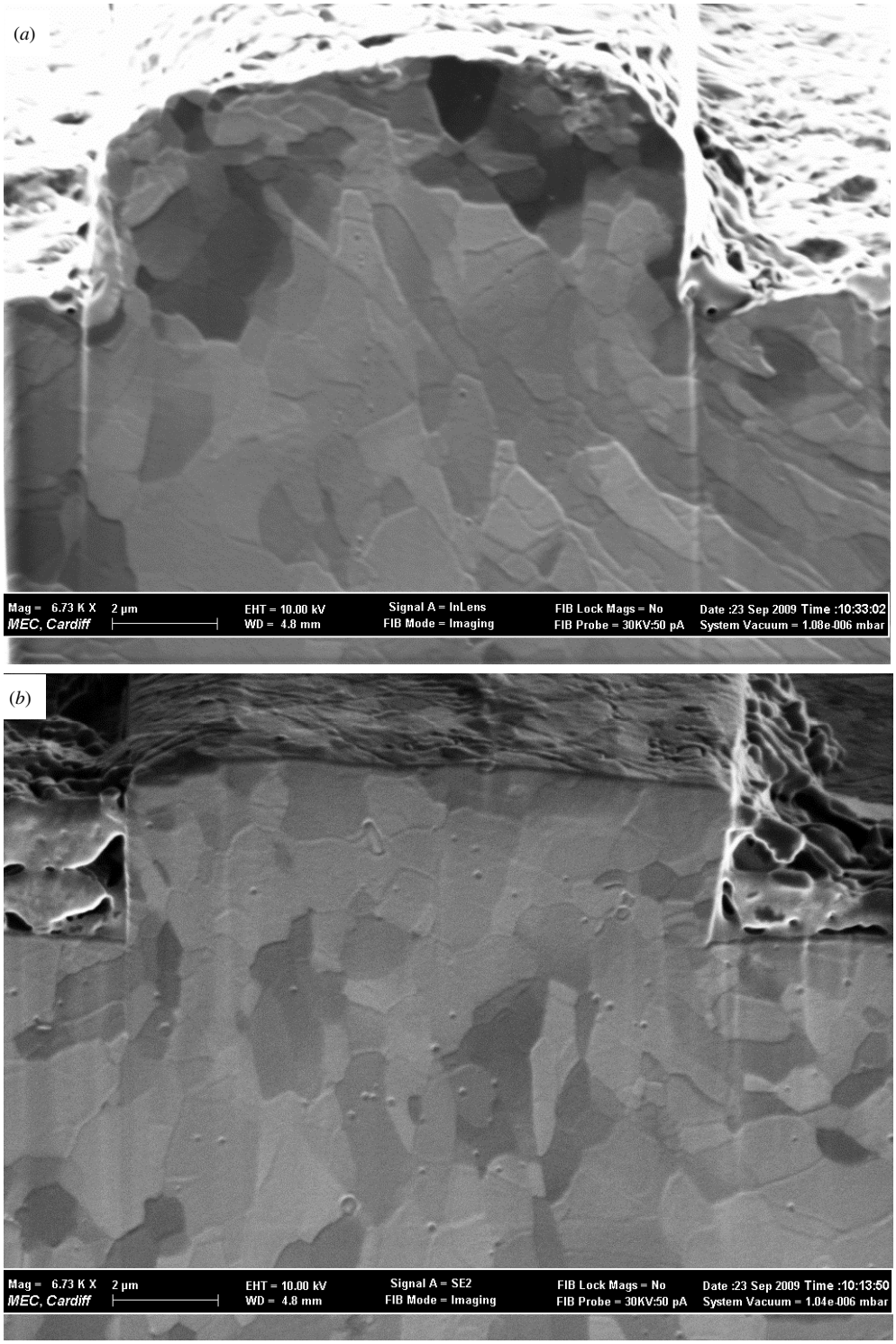

Figure 8. FIB images of the cross-section of the cold embossed Al-1050 foils processed by various passes of ECAP: (*a*) Two passes, (*b*) eight passes.

corner region of the punch; the maximum being 3.28 for condition 2 (UFG Al-1050 deformed at $T = 20\ ^{\circ}\mathrm{C}$), followed by 2.84 for condition 3 and 2.73 for condition 1 (conventional Al-1050 deformed at $T = 20\ ^{\circ}\mathrm{C}$). As expected, the maximum y-displacements occurred near the top end of the punch as it was completely pressed against the indented material. The maximum y-displacement in the indented material equalled the maximum applied displacement of 5 μm at which the punch was pressed and was recorded near the edge of the punch top end.

Figure 12 shows the contour plot of equivalent plastic strains. The contact region, between the round edge of the bottom of the punch and the Al material, underwent very high deformations. Away from this region, plastic strains were

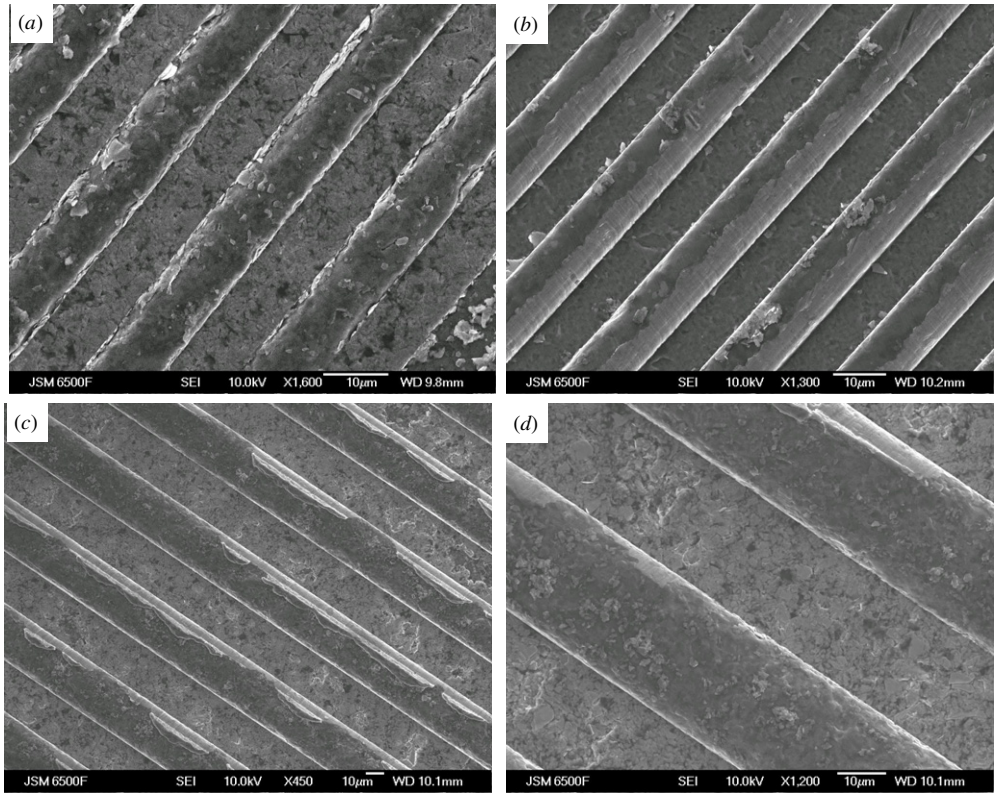

Figure 9. SEM secondary electron images showing the topography of hot embossed UFG Al samples. (*a*) UFG Al-1050 produced by four passes of ECAP—channels are 10 μm wide and 10 μm deep; (*b*) UFG Al–Mg–Cu–Mn produced by five turns of HPT—channels are 10 μm wide and 10 μm deep; (*c*) UFG Al–Mg–Cu–Mn produced by five turns of HPT—channels are 25 μm wide and 10 μm deep; (*d*) enlarged image of (*c*).

found to be less than 2.73, 10.69 and 10.72 for conditions 1, 2 and 3, respectively. The maximum plastic strains in the entire indented material were quite large: 24.61, 96.27, 2 and 96.45, respectively. At the interface between the punch right edge and the indented material, a corner gap was found in all cases even when the material was not hardening.

4. Discussion

The objective of transferring the microchannels from the micro silicon die to the Al foils is to fabricate a micro heat exchanger. The next step after embossing is to bond the embossed Al foils through diffusion bonding. A sharp channel edge is essential to obtain a good bonding quality, as a rounded edge would reduce the contact area of two Al foils during diffusion bonding producing a weaker bonding with a notch like feature, which ultimately could lead to failure and leakage. A fine grain size is crucial to obtain sharp channel edges [7].

Al alloys with addition of Mg and Cu and containing a large fraction of fine non-shearable particles have a potential to achieve an improved grain refinement during SPD [12, 35–37]. For instance, the grain size of Al-2024 (Al–4%Cu–1.5%Mg–0.4%Mn) after eight passes of ECAP can be refined to 0.3 μm [38], which is 30 times smaller than the channel depth used in this work (10 μm). Furthermore, the HPT is more powerful in grain refinement than ECAP because a more severe strain can be created, and strain can be generated without interruption. However, the size of HPT samples, although large enough for most MEMS applications, is much smaller than ECAP samples. In the present study, ultra fine grains are achieved in Al–Mg–Cu–Mn alloy processed HPT despite the fact that both cold and hot embossing were prone to processing problems.

4.1. Cold embossing process

The Al–Mg–Cu–Mn alloy processed through five turns of HPT failed to be embossed at room temperature; the hardness was too large (about 2.0 GPa) for the current press. The method outlined in [7] predicts a required embossing force of 73 kN, which is seven times larger than the press capacity of 10 kN. Using a more powerful press will not work because it will cause a significant increase of the failure rate of the micro silicon die [7].

Al-1050 was partly embossed at room temperature. Only one third of the foil surface was patterned when the embossing force was set at 5 kN, rising to about 50% when the embossing force was set to 7 kN or 9 kN. Additionally, the failure rate (breaking of silicon mould) dramatically increased when the embossing force was raised from 5 kN to 9 kN. The cross-section of the cold embossed part of Al-1050 processed by eight passes of ECAP (see figure 8(*b*)) shows a sharper edge and a flatter channel top than the Al-1050 processed by two passes of ECAP due to the smaller grain size. The cross-section profile also appears to be of trapezoidal shape with a long side on the top. This is consistent with the FE predictions:

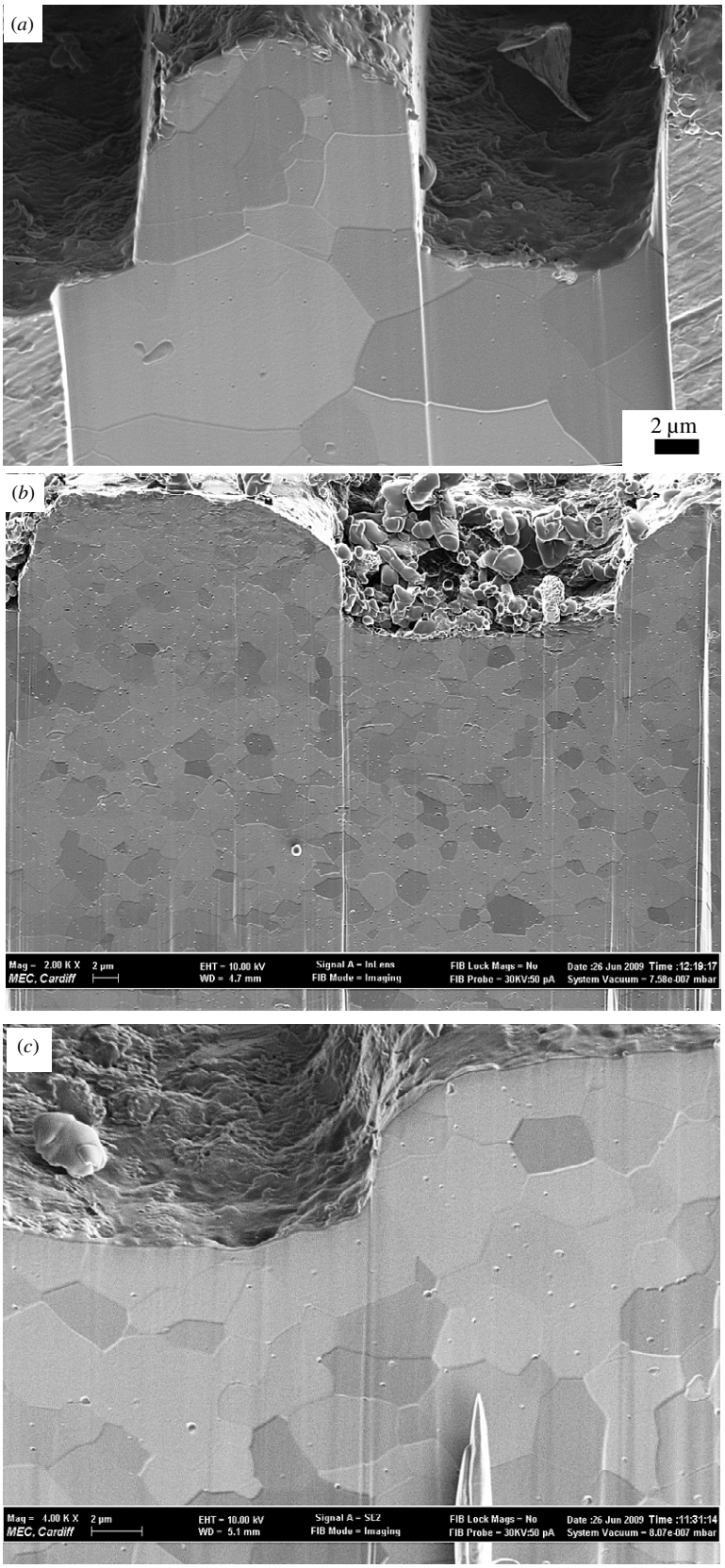

Figure 10. Secondary electron image of cross-section of hot embossed UFG Al alloys taken by FIB. (*a*) UFG Al-1050 produced by eight passes of ECAP; (*b*) UFG Al-Mg–Cu–Mn produced by five turns of HPT, the channel is 25 μm wide and 10 μm deep; (*c*) UFG Al–Mg–Cu–Mn produced by five turns of HPT, the channel is 50 μm wide and 10 μm deep.

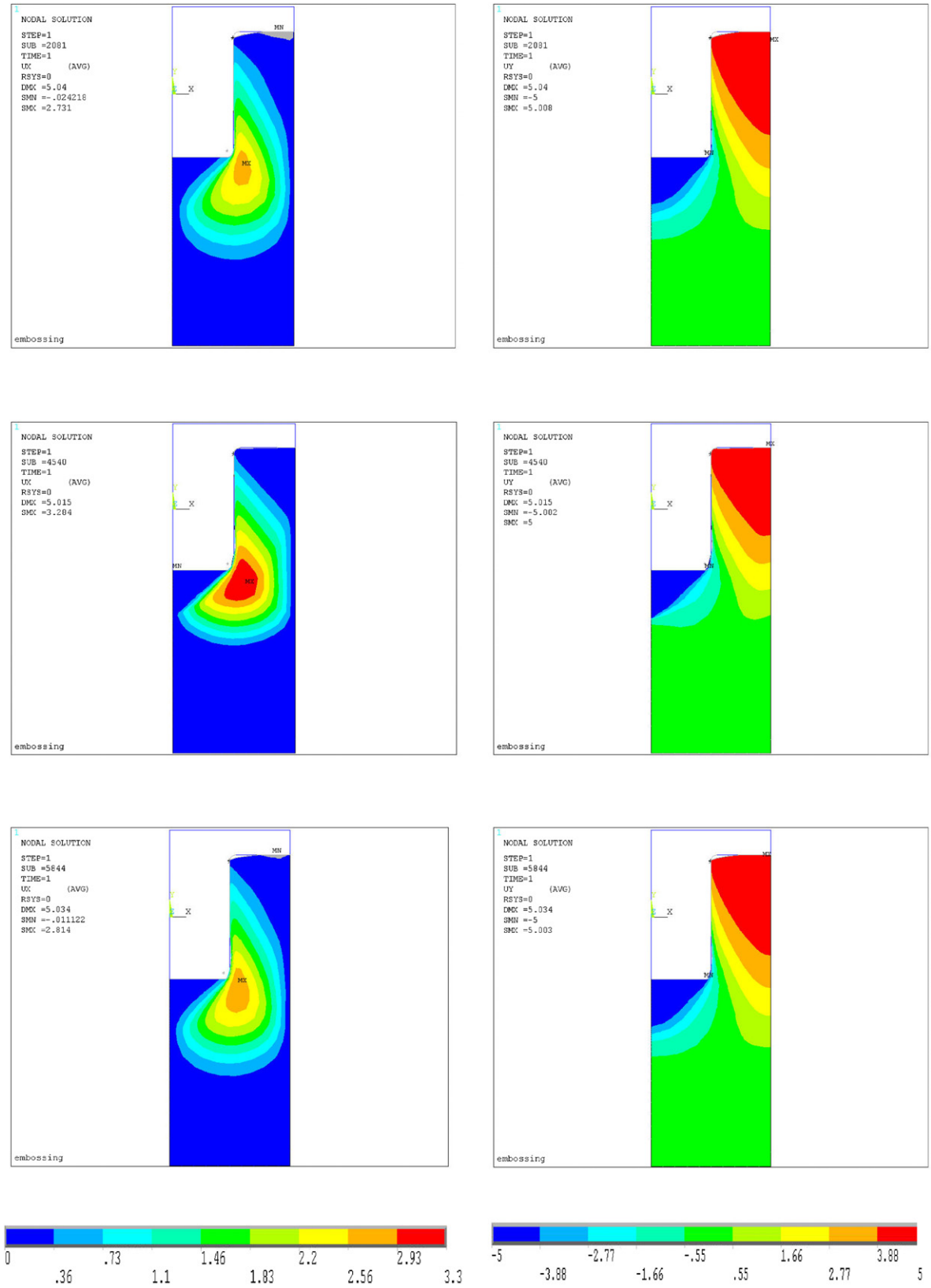

Figure 11. Contour plot of *X*-displacement (left) and *Y*-displacement (right) in indented assembly: at 20 °C before ECAP (top), at 20 °C after ECAP (middle) and at 300 °C after ECAP (bottom).

figure 12 shows a gap between the insert and the embossed Al-1050 material, i.e. around the end of the channel sidewall. The present FE study also shows that the channel top edge tends to move laterally towards the insert after demoulding to

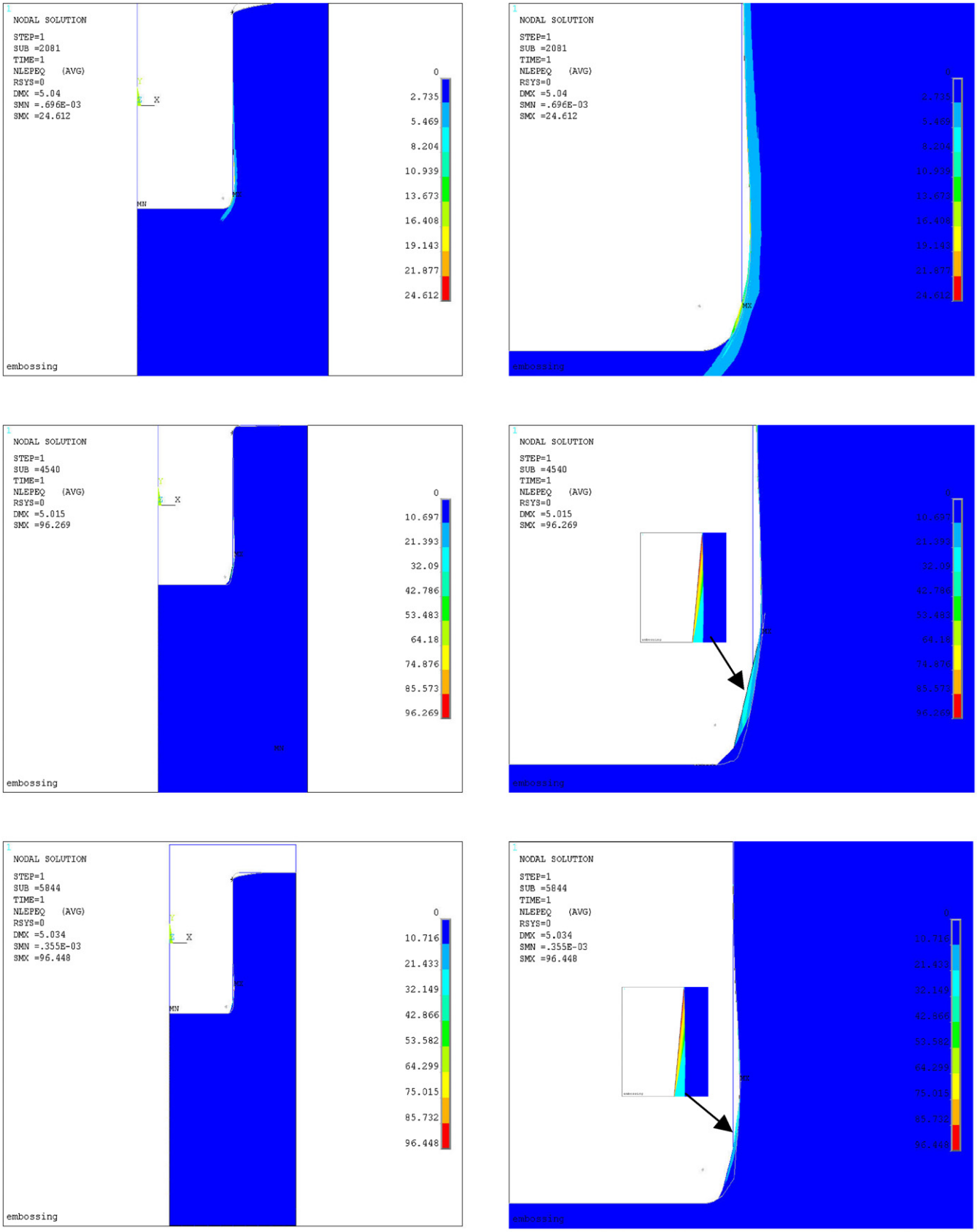

Figure 12. Contour plot of equivalent plastic strain in the indented Al alloy: entire model (left), zoomed model (right), at 20 °C before ECAP (top), at 20 °C after ECAP (middle) and at 300 °C after ECAP (bottom).

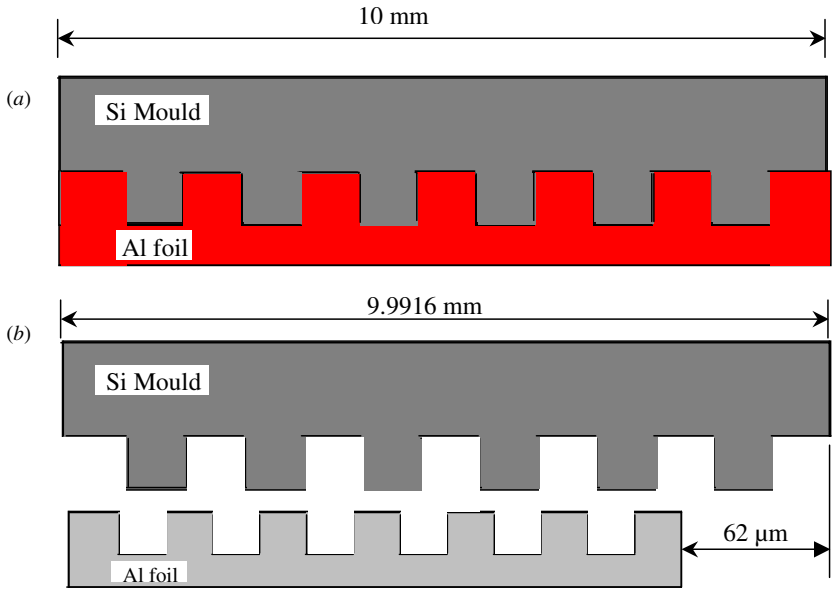

Figure 13. Schematic illustration of the thermal expansion of an Al foil and a Si mould during hot embossing and demoulding. (*a*) Embossing at 300 °C, (*b*) demoulding at room temperature.

release the large residual stress stored during embossing (see figure 11). This will cause problems for releasing the micro silicon die from the cold embossed Al foils.

4.2. Hot embossing process

During embossing at 300 °C, the pattern on the silicon die was fully transferred to the Al-1050 and Al–Mg–Cu–Mn by a reduced force of 3 kN. Small grains are thought to be crucial to obtain sharp channel edges and a flat channel top [7]. However, the HPT-processed Al–Mg–Cu–Mn with a very small grain size still has rounded channel edges after embossing at 300 °C (see figures 10(*b*) and (*c*)). It is thought that optimizing processing conditions such as loading rate and holding time may alleviate these issues. To this end, hot tensile tests or hot compression tests can be conducted at various temperatures and different strain rates. Nevertheless, the hot embossed Al foils, unlike the cold embossed ones, did show straight sidewalls of channels (see figure 10). This is supported by the FE modelling results of hot embossed Al foils. A nearly full contact is found between the embossing tool and the sidewall of channels (see figure 12), which would be favourable for releasing the mould after embossing. The reason behind is that the behaviour of Al alloys deforming at high temperature is different with that at room temperature as shown in stress–strain curves (see figure 5). Also, at high temperature, this deformation is dominated by grain rotation and grain boundary sliding, which differs from the mechanism of dislocation slip during deformation at room temperature. Moreover, the internal stress in the embossed channels generated during embossing would be recovered at least partly during holding at elevated temperature, which avoids forming a trapezoidal channel after demoulding.

The above analysis suggests that hot embossing leads to straight sidewalls of channels and easy demoulding. However, releasing the mould from the hot embossed Al foils proved more difficult than from cold embossed ones, and channel tops were scratched by the mould during demoulding (see figures 9(*b*)–(*d*)). This is because demoulding was carried out at room temperature and Al foils had much more shrinkage than the micro silicon mould. As shown in figure 13, the micro silicon mould and the Al foil are supposed to be 10 mm wide at 300 °C. Since the coefficients of linear thermal expansion for Si and Al at 20 °C are 2.6×10^{-6} °C^{-1} and 23×10^{-6} °C^{-1} [39], respectively, an unconstrained Al foil would shrink 0.6% more as compared to unconstrained Si. Thus, the embossed Al foil cooled after embossing and in contact with the Si mould should experience a tensile stress creating strong friction forces when one attempts to release it from the micro silicon mould. The stress release occurring when the Al foils detach from the micro silicon mould increases the possibility of scratching the channel top. Demoulding at the embossing temperature may avoid this shrinkage problem and will lead to a smooth mould release process. In the present study, the mould release was performed manually at room temperature, as automatic tools for hot mould release were not available.

4.3. Potential of mass fabrication of MEMS components using UFG Al via the embossing process

The application of UFG Al alloys processed by SPD in MEMS depends on both the performance of the MEMS components and the cost of the whole process. The present study has shown that UFG Al can be embossed into MEMS components with sharp and smooth channels. The embossed UFG Al foils can be produced to micro heat exchangers [7] through diffusion bonding and housing. The performance of the micro heat exchanger needs to be evaluated by checking pressure drop, leakage and heat transfer efficiency. The channels with sharp

edges and smooth and flat top surfaces provide a good base for diffusion bonding. The good bonding quality, small channel size and high thermal conductivity of UFG Al lead to high heat transfer efficiency. In summary, the current study indicates that using UFG Al produced by SPD instead of conventional aluminium alloys may result in micro heat exchangers with improved properties.

The total processing cost using the current lab based is high because many subprocesses are involved from material selection to the products of micro heat exchangers such as ECAP, lithography, DRIE, embossing, bonding and housing. However, cost will be reduced significantly if mass fabrication can be achieved. The current process can be automated and mass fabrication can be achieved if adopting the equipment with proper adjustments. It is thought that commercially available hot embossing facilities for polymer with micro scale features [40, 41] can be adapted to be suitable for UFG Al and improved demoulding systems can be fitted.

5. Conclusions

A novel process for the fabrication of a MEMS metallic component with features smaller than 10 μm and high thermal conductivity was investigated. In the first stage of processing, UFG Al-1050 and Al–Mg–Cu–Mn were produced by ECAP and HPT. Conclusions are drawn as follows.

(1) Cold embossing of the UFG Al-1050 processed by ECAP leads to a high failure rate of the micro silicon mould and an incomplete pattern transaction from the silicon mould to the foil. In contrast, the UFG Al–Mg–Cu–Mn processed by HPT fails to be embossed at room temperature due to its large hardness.

(2) The partly embossed Al-1050 at room temperature shows channels with non-flat sidewalls, which causes difficulty of demoulding. This was also captured by finite element simulations.

(3) Embossing of the UFG Al-1050 and Al–Mg–Cu–Mn at 300 °C produces smooth channels with straight sidewalls. The pattern on the micro silicon mould is fully transferred to the foil surface.

(4) Scratches on the channel top and difficulty of mould release are caused by demoulding at room temperature.

(5) Hot embossing of HPT processed UFG Al–Mg–Cu–Mn shows a good potential for application in microdevice fabrication if a proper loading rate and a superplastic temperature are identified and an automatic hot demoulding tool is available.

Acknowledgments

This work was part-funded by the Engineering and Physical Sciences Research Council under grant no EP/D00313X/1. The FIB work was funded under grant no EP/F056745/1. XGQ thanks ORSAS and School of Engineering Sciences of University of Southampton for additional studentship funding. Professor S M Spearing and Dr Liudi Jiang (University of Southampton) are gratefully acknowledged for valuable discussion. Dr Georgi Lalev (University of Cardiff) is gratefully acknowledged for FIB work.

References

[1] Chang C, Wang Y F, Kanamori Y, Shih J J, Kawai Y, Lee C K, Wu K C and Esashi M 2005 *J. Micromech. Microeng.* **15** 580–85
[2] Hardt D, Ganesan B, Dirckx M, Shoji G, Thaker K and Qi W 2005 *Innovation in Manufacturing Systems and Technology* IMST(2005)01
[3] Friedrich C R and Kang S D 1994 *Preci. Eng.* **16** 56–9
[4] Schubert K, Brandner J, Fichtner M, Linder G, Schygulla U and Wenka A 2001 *Microscale Thermophys. Eng.* **5** 17–39
[5] Brandner J J, Anurjew E, Bohn L, Hansjosten E, Henning T, Schygulla U, Wenka A and Schubert K 2006 *Exp. Therm. Fluid Sci.* **30** 801–09
[6] Bier W, Keller W, Linder G, Seidel D and Schubert K 1990 *Winter Annual Meeting of the American Society of Mechanical Engineers (Dallas, TX, USA, 25–30 November 1990)* vol 19 pp 189–97 (New York: American Society of Mechanical Engineers)
[7] Qiao X G, Gao N, Moktadir Z, Kraft M and Starink M J 2010 *J. Micromech. Microeng.* **20** 045029
[8] Otto T, Schubert A, Böhm J and Gessner T 2000 *Proc. SPIE* **4179** 96–106
[9] Jiang J, Mei F, Meng W J, Sinclair G B and Park S 2008 *Microsyst. Technol.* **14** 815–19
[10] Böhm J, Schubert A, Otto T and Burkhardt T 2001 *Microsyst. Technol.* **7** 191–95
[11] Valiev R Z, Estrin Y, Horita Z, Langdon T G, Zehetbauer M J and Zhu Y T 2006 *JOM* **58** 33–9
[12] Starink M J, Qiao X G, Zhang J and Gao N 2009 *Acta Mater.* **57** 5796–11
[13] Lee S, Utsunomiya A, Akamatsu H, Neishi K, Furukawa M, Horita Z and Langdon T G 2002 *Acta Mater.* **50** 553–64
[14] Valiev R Z, Islamgaliev R K and Alexandrov I V 2000 *Prog. Mater. Sci.* **45** 103–89
[15] Valiev R Z and Langdon T G 2006 *Prog. Mater. Sci.* **51** 881–981
[16] Gao N, Starink M J, Furukawa M, Horita Z, Xu C and Langdon T G 2005 *Mater. Sci. Eng.* A **410–411** 303–07
[17] Baretzky B *et al* 2005 *Rev. Adv. Mater. Sci.* **9** 45–108
[18] Zhilyaev A P and Langdon T G 2008 *Prog. Mater. Sci.* **53** 893–979
[19] Valiev R Z and Alexandrov I V 2002 *Ann. Chim. Sci. Mater.* **27** 3–14
[20] Xu C, Horita Z and Langdon T G 2007 *Acta Mater.* **55** 203–12
[21] Sakai G, Horita Z and Langdon T G 2005 *Mater. Sci. Eng.* A **393** 344–53
[22] Montmitonnet P, Edlinger M L and Felder E 1993 *J. Tribol.* **115** 10–14
[23] Care G and Fischer-Cripps A C 1997 *J. Mater. Sci.* **32** 5653–59
[24] Yan S L and Li L Y 2003 *Proc. Inst. Mech. Eng.* C **217** 505–14
[25] Cao D M, Jiang J, Meng W J and Sinclair G B 2007 *Microsyst. Technol.* **13** 495–501
[26] Jiang J 2007 *PhD Thesis* Louisiana State University and Agricultural and Mechanical College, USA
[27] Iwahashi Y, Wang J T, Horita Z, Nemoto M and Langdon T G 1996 *Scr. Mater.* **35** 143–46
[28] Qiao X G, Starink M J and Gao N 2009 *Mater. Sci. Eng.* A **513–514** 52–58
[29] Zhu Z and Starink M J 2008 *Mater. Sci. Eng.* A **488** 125–133
[30] Zhang J, Gao N and Starink M J 2010 *Mater. Sci. Eng.* A **527** 3472–3479
[31] ANSYS 2009 *ANSYS Theory Reference Manual Release 12.0*
[32] Wang J W, Duan Q Q, Huang C X, Wu S D and Zhang Z F 2008 *Mater. Sci. Eng.* A **496** 409–16
[33] Talamantes-Silva J, Abbod M F, Puchi Cabrera E S, Howard I C, Beynon J H, Sellars C M and Linkens D A 2009 *Mater. Sci. Eng.* A **525** 147–58

[34] Sakai G, Horita Z and Langdon T G 2005 *Mater. Sci. Eng.* A **393** 344–51
[35] Furukawa M, Utsunomiya A, Matsubara K, Horita Z and Langdon T G 2001 *Acta Mater.* **49** 3829–38
[36] Gubicza J, Chinh N Q, Horita Z and Langdon T G 2004 *Mater. Sci. Eng.* A **387–389** 55–9
[37] Wang S C, Zhu Z and Starink M J 2005 *J. Microscopy* **217** 174–78
[38] Lee S, Furukawa M, Horita Z and Langdon T G 2003 *Mater. Sci. Eng.* A **342** 294–301
[39] Kaye G W C and Laby T H 1995 *Tables of Physical and Chemical Constants* 16th edn (Harlow: Longman)
[40] Datta P and Goettert J 2007 *Microsyst. Technol.* **13** 265–70
[41] Lindner P, Glinsner T and Schaefer C 2002 *Proc. IEEE Sensors* **2** 931–35